Sensitivity Characteristics of Long-Period Fiber Gratings

Xuewen Shu, Lin Zhang, *Member, OSA*, and Ian Bennion, *Member, IEEE, Member, OSA*

***Abstract*—We present a detailed investigation into the sensitivity of long-period fiber gratings (LPFGs) as a function of temperature, strain, and surrounding refractive index, with particular attention to the higher order cladding modes and the possibilities for ultrasensitive sensors. From a general theoretical analysis, we identify a general sensitivity factor which offers new physical insight into LPFG behavior and represents a useful design aid in conjunction with a set of measurand-specific sensitivity factors. Our analysis reveals the existence of turning points in the mode dispersion characteristics at which ultrasensitive operation may be obtained. In an extensive set of coordinated experiments, we verify the theoretical predictions with close agreement and provide demonstrations of the device behavior close to the turning points. Alternative sensor schemes for temperature, strain, and refractive index based, respectively, on measurement of the dual resonance characteristic of the modes and on the transmission characteristics close to the turning points, utilizing higher order modes of the LPFG, are presented. For two variables at least, we record the highest LPFG sensitivities yet reported.**

***Index Terms*—Fiber gratings, long-period fiber gratings (LPFGs), optical fiber communication, optical fiber devices, optical fiber sensors.**

I. Introduction

LONG-PERIOD fiber gratings (LPFGs) that can couple light between the core and cladding modes of an optical fiber have become increasingly popular for applications in fiber-optic communications and sensing. The advantages of these devices include ease of fabrication, low insertion loss, low-level back reflection, and compactness. Various LPFG devices have been demonstrated for use as band rejection filters [1], erbium-doped fiber amplifer (EDFA) gain equalizers [2], comb filters [3], mode converters [4], and sensors for physical parameters such as temperature, strain, refractive index (RI), and curvature [5]–[8]. In all fields of potential application, knowledge of the sensitivity of the LPFG to the parameters of its physical environment is clearly important. For most telecommunications applications, low sensitivity is generally desirable to minimize the influence of environmental variations on device performance. For sensors, on the other hand, and for some dynamically controlled devices [9], high sensitivity is usually advantageous. Thus, whether it is with the objective of maximizing or of minimizing its value, full characterization of the sensitivity of the LPFG is an important precursor to practical device design. Although there have been several studies of this subject [1], [5]–[8], most of them have been focused on the resonant coupling of lower order cladding modes. Recently, we have found that the higher order mode resonances exhibit some quite different and potentially advantageous properties, including a dual resonance feature [10] that may be exploited to realize highly sensitive devices [11], [12]. The purpose of the work reported here is to extend the theoretical and experimental studies of LPFG sensitivity, seeking to achieve a more complete description of device behavior than has previously been presented.

This paper is constructed as follows. In Section II, we present general analytic expressions for the sensitivity of the LPFG to temperature, strain, and surrounding RI. We identify a general sensitivity factor γ and specific sensitivity factors Γ_{temp}, Γ_{strain}, and Γ_{sur}, for each of the three parameters, which offer physical insight into the LPFG behavior, as well as rather useful design aids. Theoretically, we show that the dispersion curve for each cladding mode exhibits a turning point at which maximum sensitivity of the LPFG occurs, and we go on to show that a region of ultrahigh sensitivity may be specified by $|\gamma| > 5$. The sensitivity factors are discussed in detail, supported by the results of extensive numerical simulations. In Section III, we present experimental results on the sensitivities of different resonance orders obtained from a series of LPFGs of various periods produced in boron–germanium (B–Ge) codoped fiber, validating the theoretical descriptions with extremely good accuracy, and demonstrating the value of the sensitivity factors. We demonstrate some ultrahigh-sensitivity sensors based on dual resonance measurement, or intensity measurement, around the turning points. In Section IV, we discuss issues relating to practical utilization, including the LPFG bandwidth around the turning points, and techniques to minimize cross sensitivity. Overall conclusions are given in Section V.

II. Theory and Simulation

A. General Expressions for the Sensitivities of LPFGs

An LPFG is formed typically by photoinducing a periodic refractive index modulation in the fiber core. The resulting transmission spectrum consists of distinct resonant loss bands that are due to the coupling of the fundamental core mode (LP_{01}) to the forward-propagating cladding modes (LP_{0m}). It is well known that the resonance wavelength λ_{res} of an LPFG with period Λ is determined by the phase-matching condition [1]

$$\lambda_{\mathrm{res}} = \left(n_{\mathrm{co}}^{\mathrm{eff}} - n_{\mathrm{cl},m}^{\mathrm{eff}}\right)\Lambda \tag{1}$$

Manuscript received July 2, 2001; revised October 2, 2001. This work was supported in part by the U.K. Engineering and Physical Sciences Research Council.

X. Shu was with the Photonics Research Group, Aston University, Birmingham B4 7ET, U.K. He is now with Indigo Photonics, Ltd., Birmingham B7 4BB, U.K. (e-mail: X.Shu@aston.ac.uk).

L. Zhang and I. Bennion are with the Photonics Research Group, Aston University, Birmingham B4 7ET, U.K.

Publisher Item Identifier S 0733-8724(02)00496-6.

where $n_{\rm co}^{\rm eff}$ and $n_{{\rm cl},m}^{\rm eff}$ are the effective indexes of the fundamental core mode and the mth cladding mode, respectively.

Using (1), we can derive analytic expressions for the temperature sensitivity $d\lambda_{\rm res}/dT$, the strain sensitivity $d\lambda_{\rm res}/d\varepsilon$, and the surrounding RI sensitivity $d\lambda_{\rm res}/dn_{\rm sur}$ of the resonant wavelength as

$$\frac{d\lambda_{\rm res}}{dT} = \lambda_{\rm res}\cdot\gamma\cdot(\alpha+\Gamma_{\rm temp}) \tag{2}$$

$$\frac{d\lambda_{\rm res}}{d\varepsilon} = \lambda_{\rm res}\cdot\gamma\cdot(1+\Gamma_{\rm strain}) \tag{3}$$

$$\frac{d\lambda_{\rm res}}{dn_{\rm sur}} = \lambda_{\rm res}\cdot\gamma\cdot\Gamma_{\rm sur} \tag{4}$$

where α is the thermal expansion coefficient of the fiber. γ describes the waveguide dispersion and is defined by [12], [13]

$$\gamma = \frac{\frac{d\lambda_{\rm res}}{d\Lambda}}{n_{\rm co}^{\rm eff}-n_{{\rm cl},m}^{\rm eff}}. \tag{5}$$

$\Gamma_{\rm temp}$, $\Gamma_{\rm strain}$, and $\Gamma_{\rm sur}$ describe the temperature, strain, and surrounding RI dependences, respectively, of the waveguide dispersion and are defined by

$$\Gamma_{\rm temp} = \frac{\xi_{\rm co}n_{\rm co}^{\rm eff}-\xi_{\rm cl}n_{{\rm cl},m}^{\rm eff}}{n_{\rm co}^{\rm eff}-n_{{\rm cl},m}^{\rm eff}} \tag{6}$$

$$\Gamma_{\rm strain} = \frac{\eta_{\rm co}n_{\rm co}^{\rm eff}-\eta_{\rm cl}n_{{\rm cl},m}^{\rm eff}}{n_{\rm co}^{\rm eff}-n_{{\rm cl},m}^{\rm eff}} \tag{7}$$

$$\Gamma_{\rm sur} = -\frac{u_m^2\lambda_{\rm res}^3 n_{\rm sur}}{8\pi r_{\rm cl}^3 n_{\rm cl}\left(n_{\rm co}^{\rm eff}-n_{{\rm cl},m}^{\rm eff}\right)\left(n_{\rm cl}^2-n_{\rm sur}^2\right)^{3/2}} \tag{8}$$

where $\xi_{\rm co}$, $\xi_{\rm cl}$, and $\eta_{\rm co}$, $\eta_{\rm cl}$ are the thermooptic and elastooptic coefficients of the core and cladding materials, respectively, u_m is the mth root of the zeroth-order Bessel function of the first kind, and $r_{\rm cl}$ and $n_{\rm cl}$ are the radius and refractive index of the fiber cladding, respectively.

It is both interesting and instructive to note that the factor γ relates to the sensitivity of the LPFG to all forms of external perturbation including temperature, strain and surrounding refractive index. We refer to γ as the general sensitivity factor and discuss its properties in Section III.

B. Properities of the General Sensitivity Factor γ

In order to characterize the factor γ for an LPFG, we first calculate the relationship between $\lambda_{\rm res}$ and Λ. We consider an LPFG formed in step-index single-mode fiber and using the weakly guiding approximation [14] to calculate the dispersion of the propagation constant for the fundamental core mode and the cladding modes. In the experiments described subsequently (Section III), we have used a B–Ge codoped fiber; here, we take the fiber core composition to be 9.7 m% B_2O_3 and 4.03 m% GeO_2, and the cladding to be pure silica, and we have used the Sellmeier equations to calculate the material dispersions of the core and the cladding using data given in [14]. The other parameter values used in our simulations are the core radius $r_{\rm co}=3.8\ \mu$m, the cladding radius $r_{\rm cl}=62.5\ \mu$m, and an average ultraviolet (UV)-induced core index change $\delta n = 1.4\times10^{-3}$.

Previously published work has usually restricted simulations to a relatively small wavelength range and considered only a few resonant cladding modes. In this work, we have considered the rather wider wavelength range 0.8–2.0 μm and have included a large number of cladding modes—the first 30—with calculated results, as shown in Fig. 1. For clarity, the plots for cladding mode orders $m=1$ to 10, $m=11$ to 20, and $m=21$ to 30 are shown in Fig. 1(a)–(c), respectively. In Fig. 1(a), it may be seen that the phase-matching curves for the $m=1$ to $m=7$ cladding modes exhibit a positive slope throughout the 0.8–2.0 μm wavelength range and, in Fig. 1(c), that the $m=23$ to $m=30$ cladding modes exhibit a negative slope throughout the same wavelength range. In contrast, the slopes of the curves for all other cladding modes, $m=8$ to $m=22$, change their signs from positive to negative with increasing wavelength at the points denoted by the open circles in Fig. 1. Thus, for each mode that exhibits a turning point in its phase-matching curve, a given LPFG period corresponds to two resonant wavelengths and results in coupling to a single cladding mode characterized by dual resonant peaks in its transmission spectrum. This phenomenon has been observed experimentally and is described in our previous reports [10]. The turning points occur at longer wavelengths for lower order modes, shifting to shorter wavelengths as the mode order increases. Theoretically, each cladding mode exhibits a turning point, provided that the wavelength range observed is sufficiently large [15]. At each turning point, $|d\lambda_{\rm res}/d\Lambda|\to\infty$; thus, from (5), we find that $|\gamma|\to\infty$ and that the turning points determine the condition of maximum sensitivity for each cladding mode. Generally, therefore, an LPFG can be designed to exhibit very high sensitivity for a particular wavelength by selecting a cladding mode and period at, or very close to, a turning point. For design convenience, then, we may specify a sensitive region by the condition $|\gamma|>5$, which is bounded by the dotted curves in Fig. 1.

The factor γ may also be derived as

$$\gamma = \frac{\Delta n_e}{\Delta n_g} \tag{9}$$

where $\Delta n_e = n_{\rm co}^{\rm eff}-n_{{\rm cl},m}^{\rm eff}$ is the difference in effective index between the core mode and the mth cladding mode, and $\Delta n_g = n_{\rm co}^{g}-n_{{\rm cl},m}^{g}$ is the corresponding difference in group index. The group index of the core mode is defined as $n_{\rm co}^{g}=n_{\rm co}^{\rm eff}-\lambda d(n_{\rm co}^{\rm eff}/d\lambda)$ and that of the mth cladding mode as $n_{{\rm cl},m}^{g}=n_{{\rm cl},m}^{\rm eff}-\lambda d\, n_{{\rm cl},m}^{\rm eff}/d\lambda$. Plots of Δn_g against λ for the first 30 cladding modes are given in Fig. 2. It is to be noted that, in the wavelength range 0.8–2.0 μm, Δn_g is always positive for the $m=1$ to $m=7$ cladding modes, and always negative for the $m=23$ to $m=30$ cladding modes; this is in agreement with the corresponding signs of the slopes of the phase-matching curves of Fig. 1. Because Δn_e is always positive, the sign of Δn_g is determined by that of the factor γ. The regions of $\gamma>0$ and $\gamma<0$, above and below the $\Delta n_g=0$ line, are depicted in Fig. 2. The intersections of the Δn_g curves for each cladding mode with the $\Delta n_g=0$ line define the points where $|\gamma|\to\infty$ and, thus, correspond to the turning points of Fig. 1. The high sensitivity region defined by $|\gamma|>5$ is also shown in Fig. 2 as the shaded area; the tapered shape results from the larger

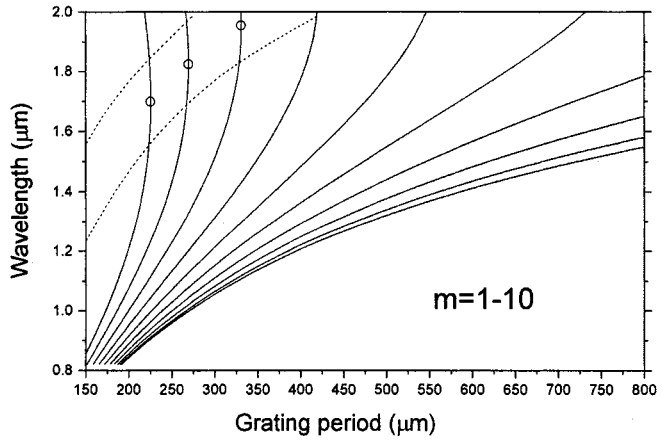

(a)

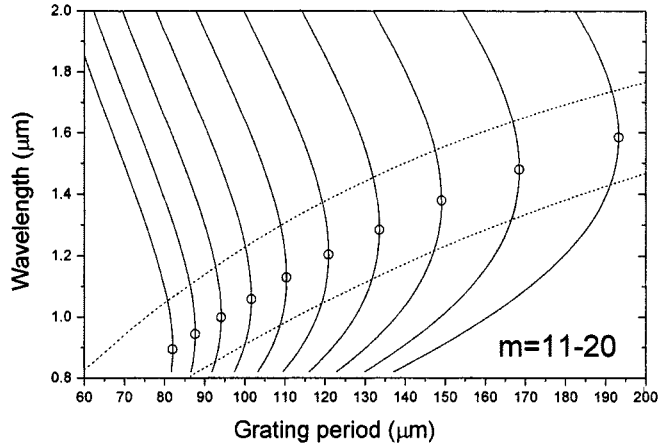

(b)

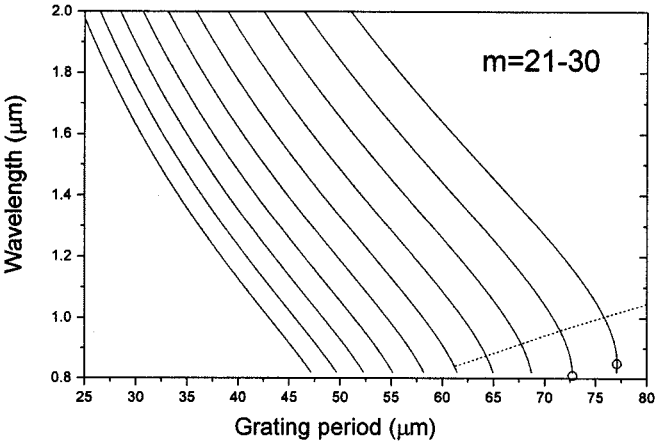

(c)

Fig. 1. Calculated variation of mode resonance wavelength $\lambda_{\rm res}$ with LPFG period Λ for B–Ge codoped fiber. (a) Modes $m = 1$ to $m = 10$. (b) Modes $m = 11$ to $m = 20$. (c) Modes $m = 21$ to $m = 30$. The small circles locate the turning points of the slopes of the curves. The two dotted lines specify the condition $|\gamma| > 5$, and in the region between these lines, the LPFG exhibits greatest sensitivity.

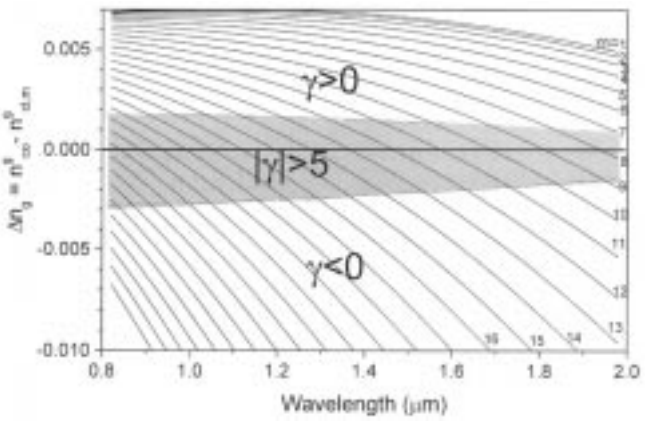

Fig. 2. Difference in group index between the fundamental core mode and each of the first 30 cladding modes (only the first 16 are numbered) as a function of wavelength, calculated for B–Ge codoped fiber. The points of intersection of the curves with the $\Delta n_g = 0$ axis correspond to the circles in Fig. 1. In the shaded region, $|\gamma| > 5$.

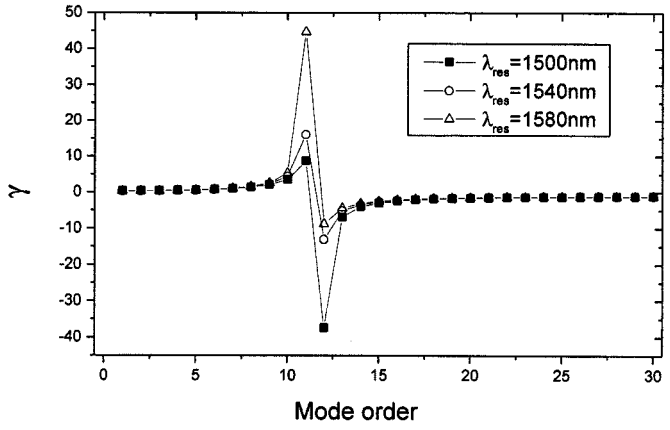

(a)

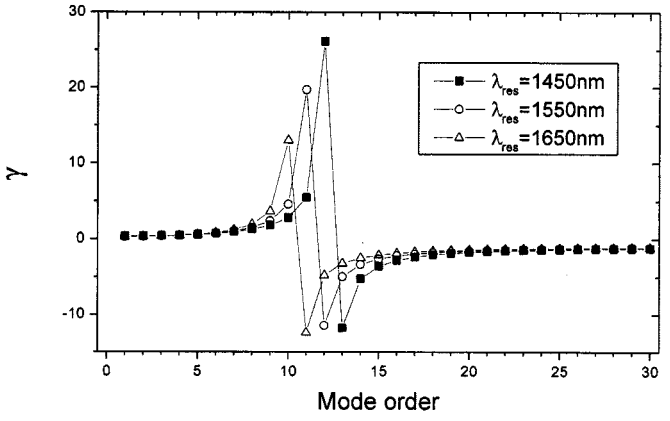

(b)

Fig. 3. Theoretical value of the general sensitivity factor γ as a function of cladding mode order for resonant wavelengths (a) $\lambda_{\rm res} = 1500$, 1540, and 1580 nm and (b) $\lambda_{\rm res} = 1450$, 1550, and 1650 nm.

values of Δn_e for longer wavelengths and higher order cladding modes.

Fig. 3 shows calculated values of γ plotted against the cladding mode order for some specific wavelengths. It is clear from the figure that the γ variations at different wavelengths exhibit a similar form characterized by a distinctive flip-flop feature around which the γ values are relatively high. This flip-flop feature was first discussed by [13] to explain the blue-shift behavior of resonances of the short period LPFGs during the UV

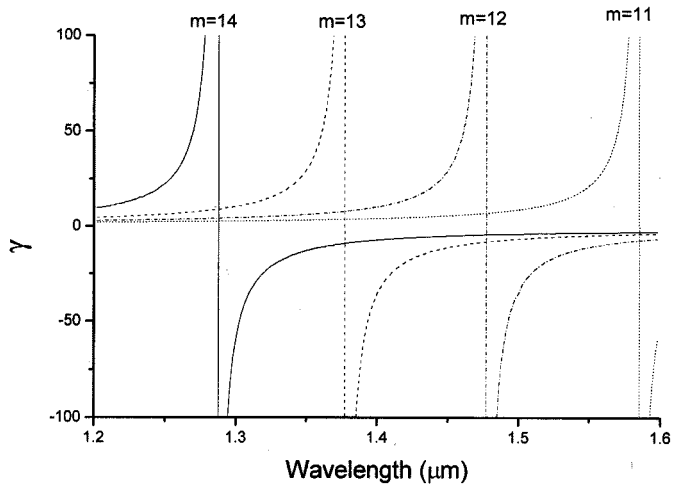

Fig. 4. γ plotted against wavelength for the $m = 11$ to $m = 14$ cladding modes. The asymptote wavelengths for each mode correspond to those at which $\Delta n_g = 0$.

exposure. Over a relatively small wavelength range, the flip-flop feature exhibits changes in the magnitude of γ only, as shown in Fig. 3(a); if the wavelength range is sufficiently large, the flip-flop feature occurs on different mode orders, as shown in Fig. 3(b).

Fig. 4 shows the calculated value of γ as a function of wavelength of the $m = 11$ through $m = 14$ cladding modes. It is evident from the figure that each mode order has two branches, corresponding to the dual resonance condition; the shorter-wavelength branch has $\gamma > 0$, and the longer-wavelength branch has $\gamma < 0$. Both branches for each mode increase rapidly in amplitude as they approach a certain wavelength, corresponding to the turning point wavelength for that mode.

C. Properties of $\Gamma_{\rm temp}$, $\Gamma_{\rm strain}$, and $\Gamma_{\rm sur}$ and Simulation Results for Sensitivities

Equations (2) to (4) show that we may separate the sensitivity of the LPFG to any given measurand into a general factor (γ) and a measurand-specific factor (Γ) that reflects the influence of the measurand on the dispersion of the LPFG.

The temperature sensitivity factor $\Gamma_{\rm temp}$ is determined by the thermooptic coefficients of the core and cladding materials, and by the mode order. Fig. 5(a) shows the variation of $\Gamma_{\rm temp}$ with mode order for a series of thermooptic coefficients. In this calculation, the thermooptic coefficient of the cladding is set to 7.8×10^{-6} for pure silica [12]. For a given value of $\xi_{\rm co}$, the absolute value of $\Gamma_{\rm temp}$ decreases with increasing mode order because Δn_e is larger for higher order cladding modes. It is to be noted also that $\Gamma_{\rm temp}$ increases with increasing difference between the thermooptic coefficients of the core and cladding materials. The sign of $\Gamma_{\rm temp}$ may be either positive or negative, as determined by $\xi_{\rm co} n_{\rm co}^{\rm eff} > \xi_{\rm cl} n_{{\rm cl},m}^{\rm eff}$ or $\xi_{\rm co} n_{\rm co}^{\rm eff} < \xi_{\rm cl} n_{{\rm cl},m}^{\rm eff}$. For standard fiber, $\Gamma_{\rm temp} > 0$, whereas for B–Ge codoped fiber, $\Gamma_{\rm temp} < 0$, because boron doping can decrease significantly the thermooptic coefficient of the core [12]. Thus, it is to be expected that the thermal responses of LPFGs produced in these two fiber types will exhibit opposite trends.

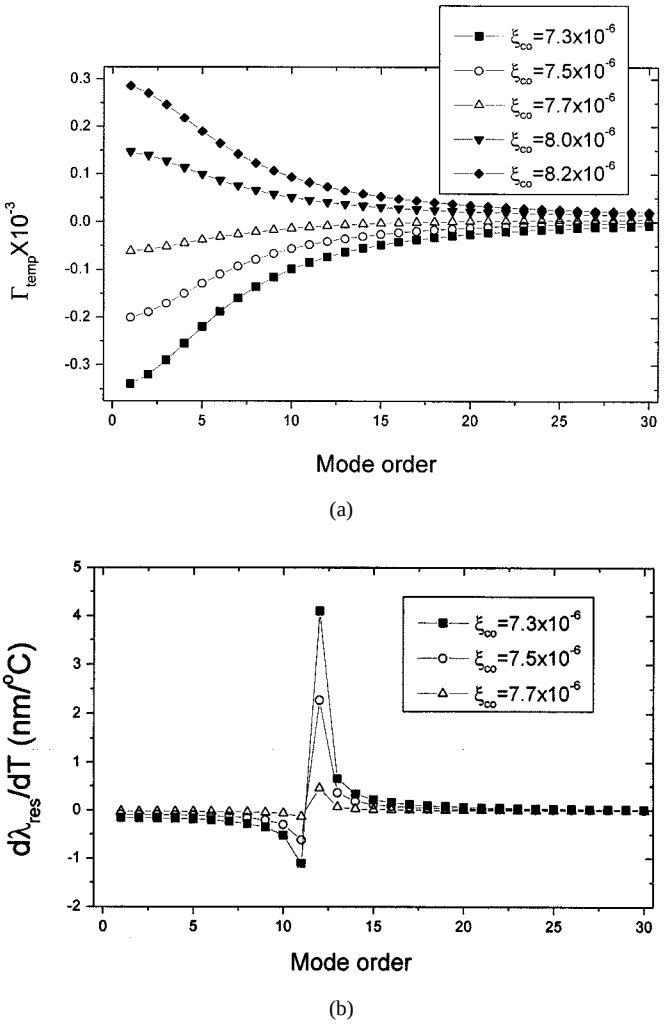

Fig. 5. Calculated values of (a) $\Gamma_{\rm temp}$ and (b) temperature sensitivity $d\lambda_{\rm res}/dT$ for the first 30 resonant cladding modes for a range of values of $\xi_{\rm co}$, with $\xi_{\rm cl} = 7.8 \times 10^{-6}$. γ values for $\lambda_{\rm res} = 1500$ nm have been used in the calculations, taken from Fig. 3.

In general, for silica-based fibers, $\alpha \ll \Gamma_{\rm temp}$, with $\alpha = 4.1 \times 10^{-7}/°$C. From (2), then, the temperature sensitivity is determined predominantly by the product $\gamma\Gamma_{\rm temp}$. However, it is necessary to consider the influence of α when designing temperature-insensitive LPFG devices. Thus, in such cases, it is not appropriate simply to satisfy the condition $\xi_{\rm co} n_{\rm co}^{\rm eff} = \xi_{\rm cl} n_{{\rm cl},m}^{\rm eff}$; rather, the condition $\Gamma_{\rm temp} = -\alpha$ should be sought.

Fig. 5(b) shows the calculated temperature sensitivity plotted against the cladding mode order for a series of values of $\xi_{\rm co}$ for LPFGs produced in B–Ge codoped fiber. [For this calculation, and for those subsequently plotted in Figs. 6(b) and 7(b), a resonance wavelength of 1500 nm is used and the value of γ is taken from Fig. 3(a).] The temperature sensitivity for each value of $\xi_{\rm co}$ is found to switch from negative to positive at the $m = 11$ and $m = 12$ modes, where it is also at its greatest. Fig. 5(b) suggests that the LPFG sensitivity may be optimized by increasing the difference between the core and cladding thermooptic coefficients and by judicious choice of resonant mode.

The strain sensitivity factor $\Gamma_{\rm strain}$ is determined by the elastooptic coefficients of the core and cladding materials, and by

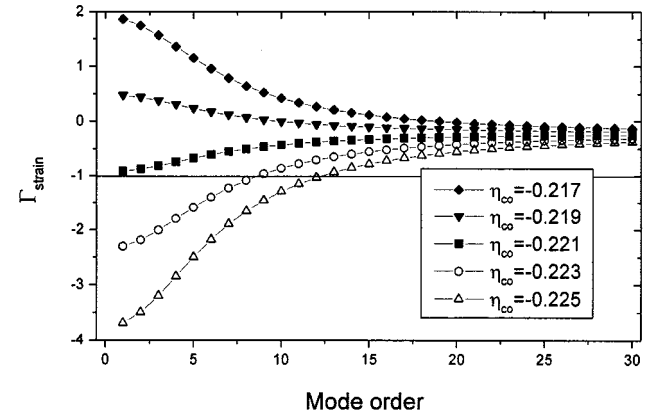

(a)

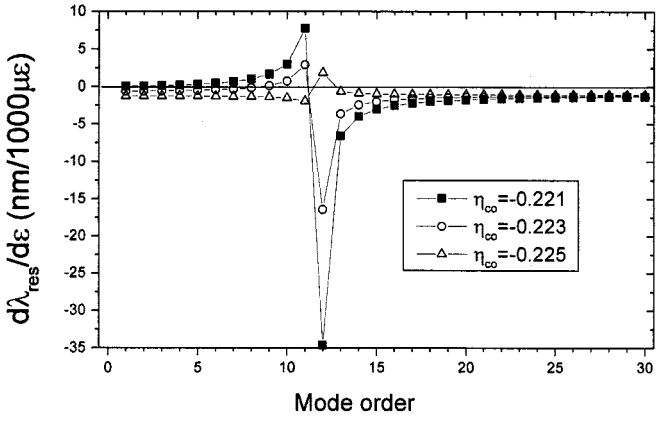

(b)

Fig. 6. Calculated values of (a) $\Gamma_{\rm strain}$ and (b) strain sensitivity $d\lambda_{\rm res}/d\varepsilon$ for the first 30 resonant cladding modes for a range of values of $\eta_{\rm co}$, with $\eta_{\rm cl} = -0.22$. γ values for $\lambda_{\rm res} = 1500$ nm have been used in the calculations, taken from Fig. 3.

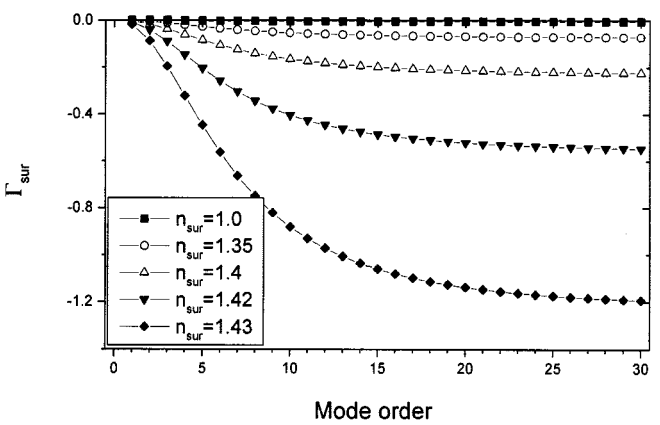

(a)

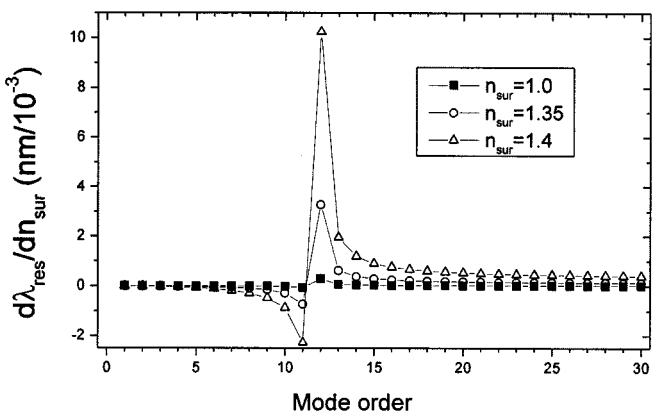

(b)

Fig. 7. Calculated values of (a) $\Gamma_{\rm sur}$ and (b) surrounding refractive index sensitivity $d\lambda_{\rm res}/dn_{\rm sur}$ for the first 30 resonant cladding modes for a range of values of $n_{\rm sur}$. γ values for $\lambda_{\rm res} = 1500$ nm have been used in the calculations, taken from Fig. 3.

the mode order. Fig. 6(a) shows the variation of $\Gamma_{\rm strain}$ with mode order for a range of values of $\eta_{\rm co}$, with $\eta_{\rm cl}$ held constant at a value of -0.22 for the pure silica cladding. As with $\Gamma_{\rm temp}$, the magnitude of $\Gamma_{\rm strain}$ decreases with increasing mode order. However, as shown by (3), the sign of the strain sensitivity $d\lambda_{\rm res}/d\varepsilon$ is determined by $\Gamma_{\rm strain} > -1$ or $\Gamma_{\rm strain} < -1$, as well as by the sign of γ; this is responsible for the relatively complicated behavior of the calculated strain sensitivity plotted against mode order in Fig. 6(b). We observe in Fig. 6(b) that although the flip-flop feature occurs at the eleventh to thirteenth modes, the behavior at $\eta_{\rm co} = -0.225$ differs markedly from that of $d\lambda_{\rm res}/dT$. Thus, $d\lambda_{\rm res}/d\varepsilon$ is seen to switch to positive at the $m = 12$ mode, and back to negative at the $m = 13$ mode. The explanation for this behavior stems from the relative signs of $\Gamma_{\rm strain}$ and γ. For $\eta_{\rm co} = -0.225$, $\Gamma_{\rm strain} < -1$ for all modes up to $m = 12$ and, thus, the signs of $d\lambda_{\rm res}/d\varepsilon$ and γ are opposite for these modes; when γ switches from positive to negative at $m = 12$, $d\lambda_{\rm res}/d\varepsilon$ switches in the opposite direction. For $m \geq 13$, $1 + \Gamma_{\rm strain} > 0$, and $d\lambda_{\rm res}/d\varepsilon$ switches once again from positive to negative. Because $\Gamma_{\rm strain} \sim -1$ at the flip-flop mode orders with $\eta_{\rm co} = -0.225$, the value of $d\lambda_{\rm res}/d\varepsilon$ for these orders is significantly smaller than with $\eta_{\rm co} = -0.221$ or -0.223. It is interesting to note that despite its value lying closer to $\eta_{\rm cl}$, $\eta_{\rm co} = -0.221$ offers greatest strain sensitivity. To produce strain-insensitive LPFGs, the condition $\Gamma_{\rm strain} = -1$ should be satisfied; this is usually possible for only one mode of the device.

In Fig. 7(a), the calculated sensitivity factor for the refractive index of the surrounding medium, $\Gamma_{\rm sur}$, is plotted against the mode order for several values of $n_{\rm sur}$. In contrast with the behaviors of $\Gamma_{\rm temp}$ and $\Gamma_{\rm strain}$, $\Gamma_{\rm sur}$ is always negative, as shown by (8). (Note that we restrict discussion in this paper to $n_{\rm sur} < n_{\rm cl}$.) For a given value of $n_{\rm sur}$, the magnitude of $\Gamma_{\rm sur}$ first increases rapidly with increasing mode order, reaching near-saturation for $m \geq \sim 20$, and is substantially larger at higher $n_{\rm sur}$. The variation of $d\lambda_{\rm res}/dn_{\rm sur}$ is shown in Fig. 7(b). In this case, the behavior is quite straightforward because the sign of $d\lambda_{\rm res}/dn_{\rm sur}$ is dependent only on that of γ. $d\lambda_{\rm res}/dn_{\rm sur}$ is negative for lower order modes, and positive for higher order modes. We note that the sensitivity is rather greater for higher order modes, in keeping with the corresponding behavior of $\Gamma_{\rm sur}$. From (8), it can be observed that $d\lambda_{\rm res}/dn_{\rm sur}$ may be significantly enhanced by reducing the cladding radius $r_{\rm cl}$, since $\Gamma_{\rm sur} \propto r_{\rm cl}^{-3}$, and this has been verified experimentally by Chiang *et al.* by measurement of the response of an etched LPFG [16].

TABLE I
SET OF LPFGS FABRICATED IN B–GE CODOPED PHOTOSENSITIVE FIBER TO GENERATE RESONANCE AROUND 1500 NM AND THEIR MEASURED TEMPERATURE, SRI, AND STRAIN SENSITIVITIES

Λ (μm)	m	λ_{res} (nm)	$d\lambda_{res}/dT$ (nm/°C)	$d\lambda_{res}/d\varepsilon$ (nm/1000με)	$d\lambda_{res}/dn_{sur}$ ($nm/10^{-3}$)
700	2	1506.3	-0.327	0.204	-0.003
620	3	1484.9	-0.35	0.347	-0.006
550	4	1492.4	-0.369	0.57	-0.019
400	6	1524.0	-0.493	1.0	-0.008
325	7	1467.0	-0.579	1.34	-0.158
254	9	1468.7	-0.497	2.69	-0.209
240	10	1530.1	-1.75	7.43	-0.819
202	11	1510.2	-1.854	30.31	-1.481
173	12	1535.8	1.64	-19.61	1.175
151	13	1535.3	0.861	-7.11	0.889
129	14	1537.1	0.543	-5.18	0.876
118	15	1511.9	0.427	-4.66	0.669
110	16	1523.8	0.377	-3.82	0.583
78	20	1442.7	0.212	-2.88	0.403
34	30	1502.0	0.075	-1.89	0.239

* $d\lambda_{res}/dT$ is measured in the temperature range of 0-60 °C; $d\lambda_{res}/d\varepsilon$ is measured in the strain range of 0-1000με; $d\lambda_{res}/dn_{sur}$ is measured in the SRI range of 1-1.36.

III. EXPERIMENTS

A. Comparison of Sensitivities of Different Resonant Mode Orders

For these investigations, a set of LPFGs with small, medium, and large periods aimed to generate resonances at a wavelength around 1500 nm were inscribed in hydrogen-free B–Ge co-doped fiber. All gratings had an approximate length of 5 cm, and were annealed at 110 °C for 24 h subsequent to UV exposure. Their spectral profiles were measured using a broad-band light-emitting diode (LED) and an optical spectrum analyzer with 0.1-nm resolution. For each LPFG, the period, the resonant wavelength that lies closest to 1500 nm in air at room temperature ,and its corresponding mode order are listed in Table I. All wavelength differences among those listed are less than 100 nm, and this permits us to make an approximate comparison of their sensitivities. In Table I, $d\lambda_{\rm res}/dT$ is measured in the temperature range of 0 °C–60 °C. $d\lambda_{\rm res}/d\varepsilon$is measured in the strain range of 0–1000 $\mu\varepsilon$. $d\lambda_{\rm res}/dn_{\rm sur}$ is measured in the surrounding medium refractive index (SRI) range of 1–1.36. As shown in Fig. 8, we have compared the experimentally determined values of the cladding-mode order against the grating period that produces a resonance at 1500 nm with the theoretically derived values; good agreement is apparent.

The LPFG thermal response was measured by heating each grating between 0 °C and 60 °C in 10 °C incremental steps using a thermoelectric cooler. The temperature sensitivity $d\lambda_{\rm res}/dT$, measured at the resonance of each LPFG, is given in Table I and plotted in Fig. 9(a). The flip-flop feature is clearly visible and attains a maximum negative value of $-1.854nm/°$C for the $m = 11$ mode in a 202-μm period grating, and a maximum positive value of 1.640 nm/°C for the $m = 12$ mode in a 173-μm period grating. Clearly, there is excellent agreement between the experimentally observed and theoretically predicted behavior.

The strain sensitivity of each grating was determined at steps of approximately 200 $\mu\varepsilon$ in the range of 0–1000 $\mu\varepsilon$ with the grating fixed between two micrometer-driven translation stages. Once again, the measured sensitivities are listed in Table I and plotted in Fig. 9(b). It is found that $d\lambda_{\rm res}/d\varepsilon$ exhibits the anticipated flip-flop behavior, changing sign from positive at the $m = 11$ mode to negative at the $m = 12$ mode, which is very close to the theoretical prediction for $\eta_{\rm co} = -0.221$ [see Fig. 6(b)].

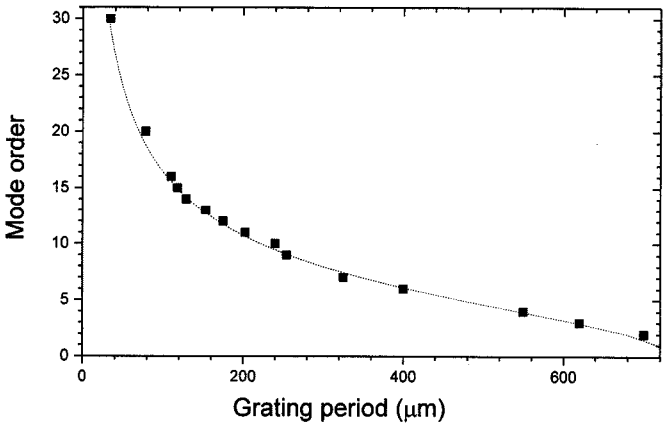

Fig. 8. Cladding mode order plotted against grating period for $\lambda_{\rm res} = 1500$ nm: comparison between experimental (black squares) and theoretical (dotted line) values.

The LPFG sensitivity to external refractive index was determined simply by comparing the resonant wavelengths in air ($n_{\rm sur} = 1.00$) and alcohol ($n_{\rm sur} = 1.36$). The values of $d\lambda_{\rm res}/dn_{\rm sur}$ averaged in the index range 1.00–1.36 for each resonance are listed in Table I and plotted in Fig. 9(c). The flip-flop feature, with $d\lambda_{\rm res}/dn_{\rm sur}$ switching from negative ($m = 11$) to positive ($m = 12$), was obtained, and it confirms the simulated prediction of Fig. 7(b). It is also apparent that the higher order modes ($m > 12$) exhibit somewhat higher sensitivity than the lower order ($m < 9$) modes, again in agreement with the theory.

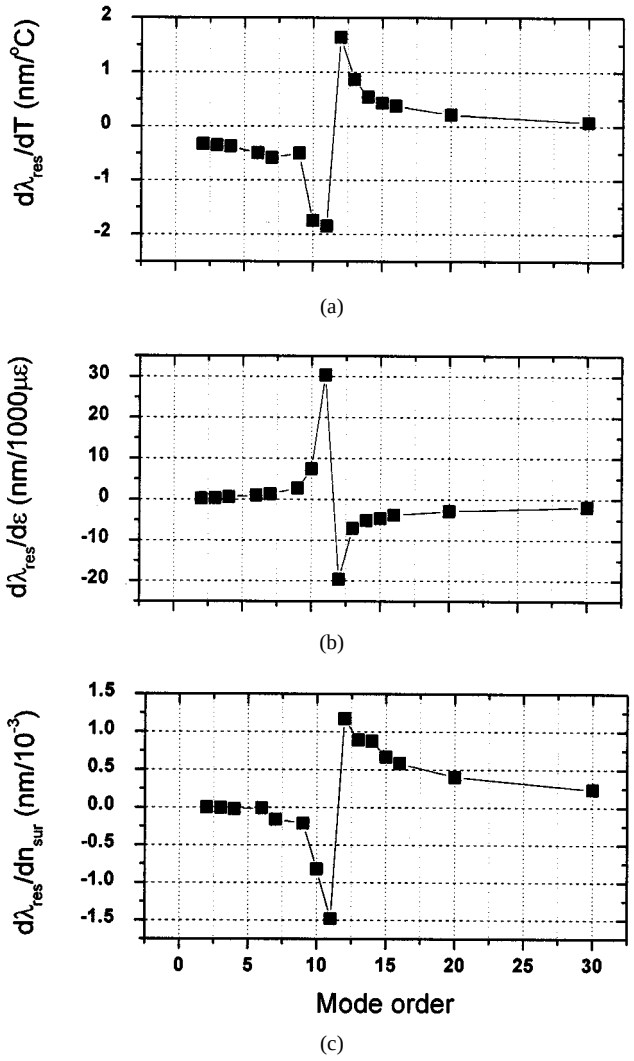

Fig. 9. Experimentally measured values of (a) $d\lambda_{\rm rcs}/dT$, (b) $d\lambda_{\rm rcs}/d\varepsilon$, and (c) $d\lambda_{\rm rcs}/dn_{\rm sur}$ plotted against cladding mode order for resonances close to $\lambda_{\rm rcs} = 1500$ nm.

B. Evidence for the Existence of the Turning Points

From the theory presented in Section II-B, it is anticipated that dual resonant peaks will be observed in the coupling of the core mode to a single cladding mode in the LPFG, provided that the grating period is smaller than, but close to, that of a turning point. Thus, observation of the dual resonance may be used to identify the location of a turning point. Experimental observation of this feature may be made during the LPFG inscription process, via postfabrication exposure [10], or in a sensing measurement. Here, we present observations made during the inscription process.

Fig. 10 presents evidence of the existence of the turning points recorded during the fabrication of a series of LPFGs in B–Ge codoped fiber. Fig. 10(a)-(f) shows results for six individual gratings; the grating periods were 202.5, 175, 153, 133, 120, and 109 μm, respectively, chosen to generate dual resonances with corresponding mode orders from $m = 11$ to $m = 16$, respectively. It is clear, from Fig. 10, that each grating has indeed generated a dual-peaked resonance for a specific mode order, as depicted by the solid line traces. With further UV exposure (note that overexposure can weaken the resonant coupling), in each case, the two peaks moved closer to each other and eventually coalesced, as shown by the dashed line traces in Fig. 10. The peak wavelength of each coalesced dual resonance corresponds to that of the turning point specified in Section II-B. It is also clear from these experiments that the turning points occurred at shorter wavelengths with increasing mode order. We note that the progressively weaker coupling strength to the dual peaks as m increases is due to the corresponding decrease in the overlap between the core and cladding field distributions.

The theoretically predicted (hollow circles) and experimentally measured (solid squares) wavelengths of the turning points for $m = 10$ through $m = 18$ cladding modes are presented in Fig. 11. We find that the experimental results for the $m = 10$ through $m = 13$ cladding modes show good agreement with the simulations presented in Section II, which were based on our usual value for this fiber of $\delta n = 0.0014$ for the average UV-induced refractive index change in the core. However, the rather longer exposure times necessary to induce the higher order mode resonances render this figure inaccurate for $m > 13$. We have recalculated the turning point wavelengths with the assumption of a larger $\delta n = 0.0022$; the results are also shown in Fig. 11 (hollow triangles). It may be seen that the experimental data for the $m = 14$ through $m = 18$ modes show close agreement with the recalculated simulation.

C. Ultrasensitive LPFG Sensors Employing Dual Resonance

The results presented in Section III-B indicate that, with appropriate design for operation near the turning points, highly sensitive LPFG-based sensors for temperature, strain, or refractive index may be conceived. Here, we present some experimental results that support this conclusion.

1) Temperature Sensors: Fig. 12 shows results obtained for a number of temperature sensors employing the dual resonance feature of the LPFG. In Fig. 12(a), curve 1 shows the measured response of the $m = 11$ cladding mode of a 202.5-μm period LPFG over the temperature range 0–80 °C. At a temperature of 0–10 °C, the mode exhibits a single resonance that is wavelength-independent of temperature. At 20 °C, the single mode has bifurcated and shows two resonances separated by 66.6 nm (red shift $+32.4$ nm, blue shift -34.2 nm). The two resonances continue to separate with increasing temperature, reaching a separation of 268.9 nm (red shift $+123.5$ nm, blue shift -145.4 nm) at 80 °C. If we utilize the wavelength separation as the basis of temperature measurement, the device exhibits a sensitivity as large as 3.4 nm/°C in the 20 °C–60 °C range. Curves 2 and 3 in Fig. 12(a) illustrate two further examples, the response of the $m = 12$ mode of a 175-μm period grating, and of the $m = 13$ mode of a 153-μm grating, respectively. Apart from the wavelength separation occurring at a different temperature, these responses are similar to that of curve 1. For the 175-μm period device, the wavelength separation increases from 92.0 nm at 30 °C to 253.2 nm at 80 °C; for the 153-μm period device, the separation is 103.6 nm at 30 °C, increasing to 247.8 nm at 80 °C. In all cases, the magnitudes of the blue-shifted resonances are slightly greater than those

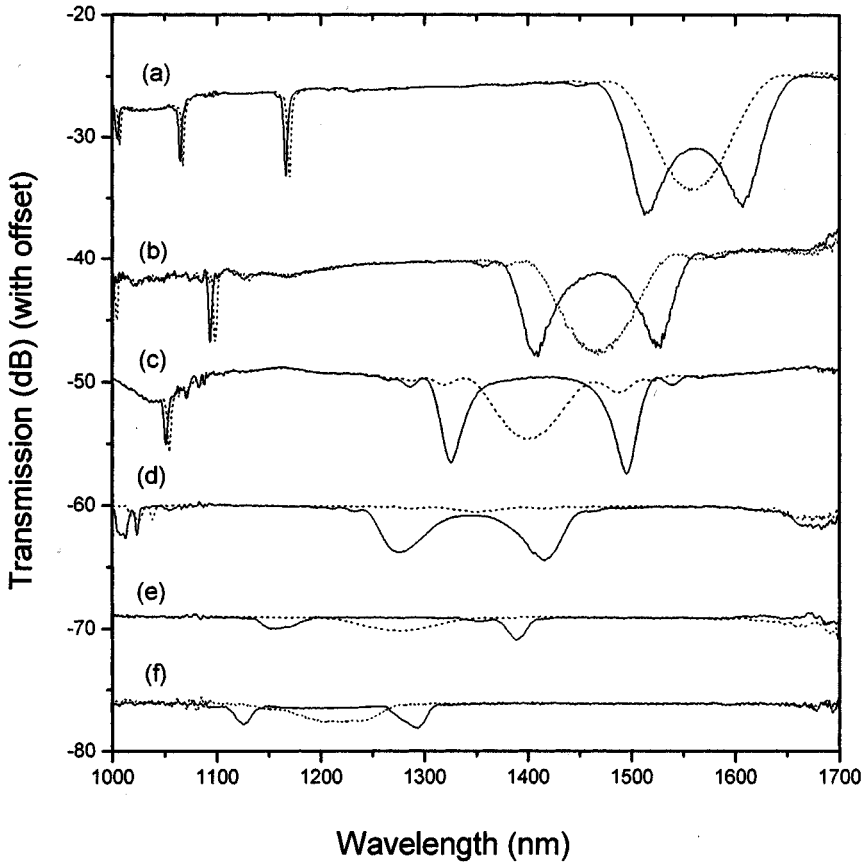

Fig. 10. Transmission spectra for six LPFGs measured during the UV inscription process. For a particular mode in each case (see text), the dual resonance peaks (solid line) were observed to coalesce in a single peak (dashed line). The grating periods were (a) 202.5 μm, (b) 175 μm, (c) 153 μm, (d) 133 μm, (e) 120 μm, (f) 109 μm.

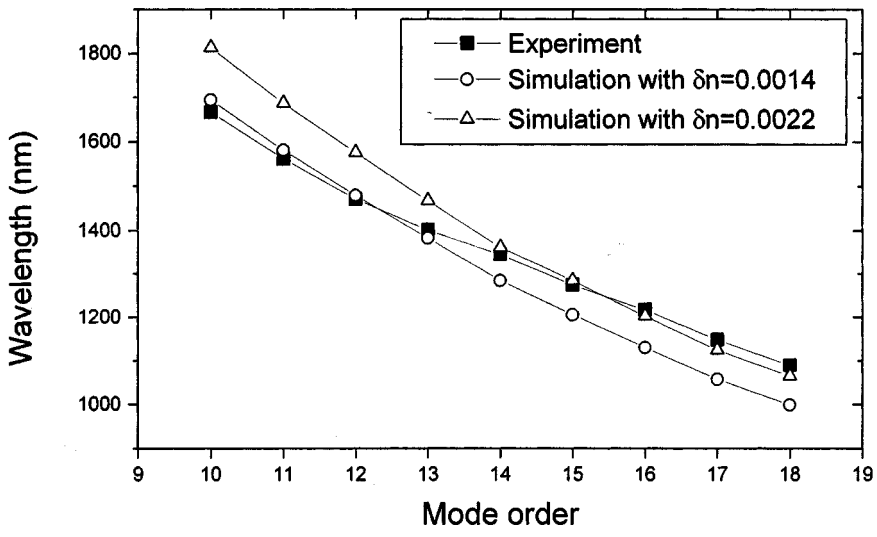

Fig. 11. Measured (solid squares) and calculated (hollow circles and triangles) wavelengths of the turning points for the $m = 10$ to $m = 18$ cladding modes.

of the red-shifted resonances. Fig. 12(b) illustrates the evolution of the transmission spectra measured for the 175-μm period device. It is clear from this figure that the dual resonance of the $m = 12$ mode is very much more sensitive to temperature (3.2 nm/°C) than is the resonant peak of the $m = 11$ mode at $\sim$1100 nm (-0.31 nm/°C).

It is apparent, from Fig. 12(a), that the temperature response is nonlinear, decreasing as the dual resonance moves further from the turning point. For the $m = 11$ mode of the 202.5-μm device, for example, the average sensitivities of each of the two peaks of the dual resonance are $+2.54$ nm/°C and -3.29 nm/°C, respectively, in 10 °C–20 °C, falling to

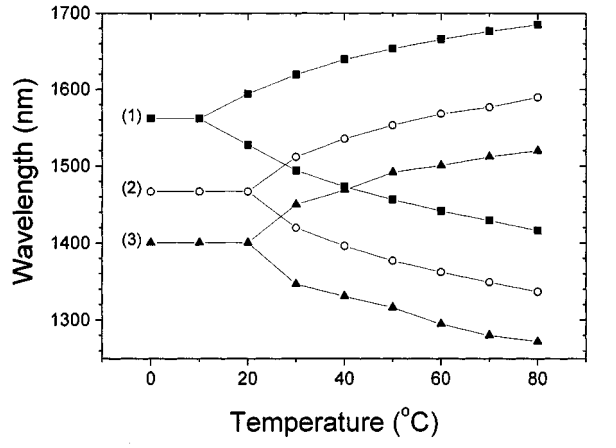

(a)

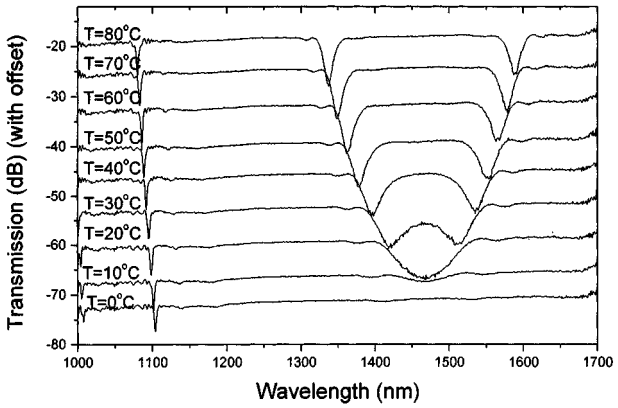

(b)

Fig. 12. Measured temperature responses of LPFGs. (a) Temperature-dependent wavelength variations of (curve 1) $m = 11$ mode, $\Lambda = 202.5$ μm grating, and (curve 2) $m = 12$ mode, $\Lambda = 175$ μm grating, and (curve 3) $m = 13$ mode, $\Lambda = 153$ μm grating. (b) Transmission spectrum of the $\Lambda = 175$ μm grating at different temperatures.

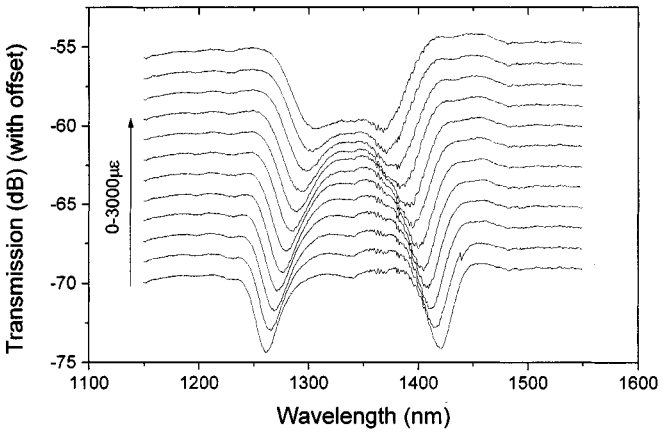

(a)

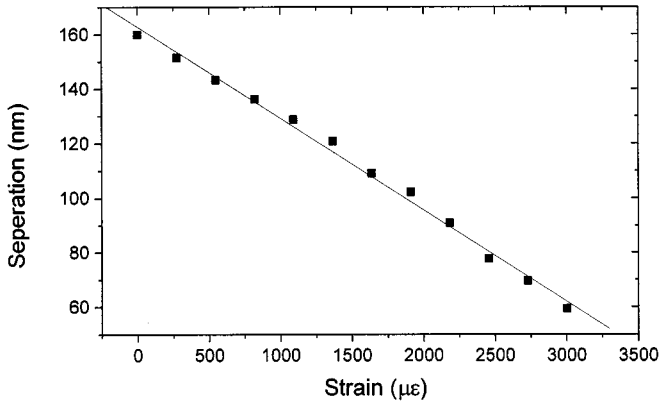

(b)

Fig. 13. Measured strain response of 133-μm period LPFG. (a) Transmission spectrum with increasing strain. (b) Separation of dual resonance peaks plotted against strain.

$+0.88$ nm/°C and -1.31 nm/°C, respectively, in 70 °C–80 °C. The origin of the nonlinearity is readily visible in Fig. 4, which shows the magnitude of γ for each mode rapidly reducing for wavelengths away from the turning point.

2) Strain Sensors: Fig. 13 illustrates a highly sensitive strain measurement based on measurement of the dual resonance separation in a 133-μm period LPFG. Fig. 13(a) shows the transmission spectra as strain is increased from 0 to 3000 $\mu\varepsilon$; the individual resonance peaks move closer together with increasing strain. The wavelength separation is plotted as a function of strain in Fig. 13(b). The sensitivity, $d\lambda_{\text{res}}/d\varepsilon$, calculated from the slope of the best fit straight line through the measured data is -33.6 nm/1000 $\mu\varepsilon$. Although the strain response is near linear, the presence of a small nonlinearity is apparent in the figure.

3) Refractive Index Sensors: The results of measurements using the dual resonance feature as a sensor for the SRI are presented in Fig. 14. In Fig. 14(a), curves 1 and 2refer to the $m = 12$ mode of the 175-μm period LPFG, and the $m = 13$ mode of the 153-μm period LPFG, respectively. The responses of the two devices to changing SRI are very similar, but for the difference in wavelength. In both cases, the resonant mode exhibited a single peak in air, and increasing bifurcation into separating peaks as the SRI was increased, the rate of separation increasing rapidly with SRI. In each case, the blue-shifted resonance is less sensitive than its red-shifted counterpart; for example, for the 153-μm LPFG, the wavelength of the blue-shifted resonance is shifted by -164.8 nm for an SRI increase from 1 to 1.44, whereas that of the red-shifted resonance is more than $+300$ nm and out of the measurement range. This sensitivity difference is not unexpected because it exhibits a λ^4 dependence, as is evident from (4) and (8). Fig. 14(b) shows the transmission spectra obtained with the 153-μm period device. It is clear from this figure that the dual resonance peaks of the $m = 13$ mode are significantly more sensitive (by more than an order of magnitude) to changing SRI than is the $m = 12$ mode at $\sim$1050 nm, which exhibits a wavelength shift of just -13.1 nm for an SRI increase from 1 to 1.44.

D. LPFG Sensors Based on Intensity Measurement

The LPFG sensors discussed above all rely on a measurand-induced change of resonant wavelength. However, an alternative sensor scheme exists; for LPFGs designed to operate at the turning point but a little off resonance, external perturbations induce only a variation in the coupling efficiency, and the maximum coupling wavelength remains constant. Here, we illustrate this principle applied to sensors for temperature and strain.

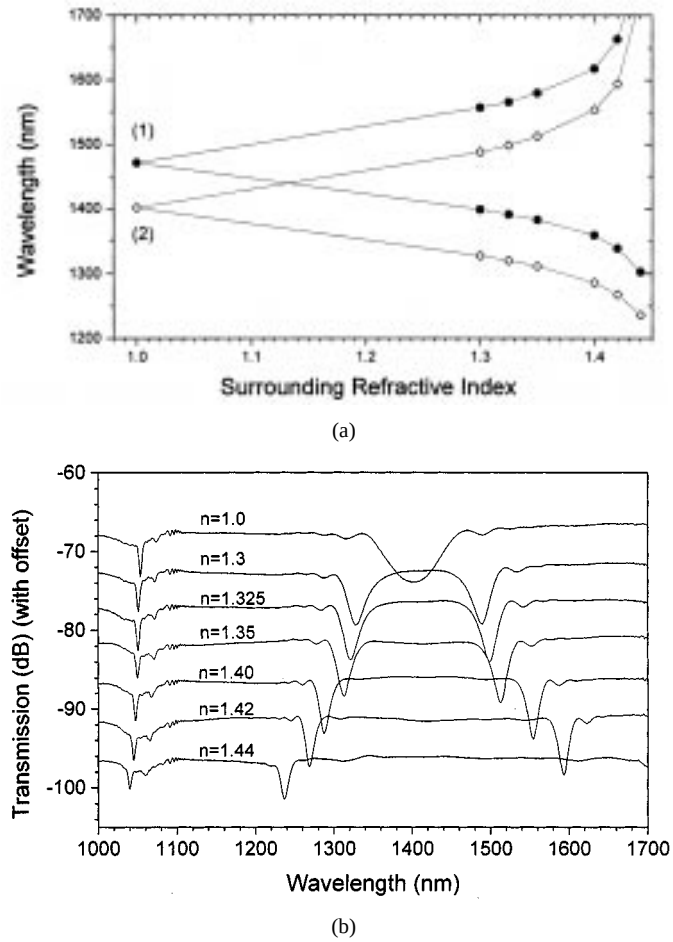

Fig. 14. Measured responses of LPFGs to SRI variation. (a) SRI-dependent wavelength variations of (curve 1) $m = 12$ mode, $\Lambda = 175\ \mu$m grating, and (curve 2) $m = 13$ mode, $\Lambda = 153\ \mu$m grating. (b) Transmission spectrum of the $\Lambda = 153\ \mu$m grating for different values of the SRI.

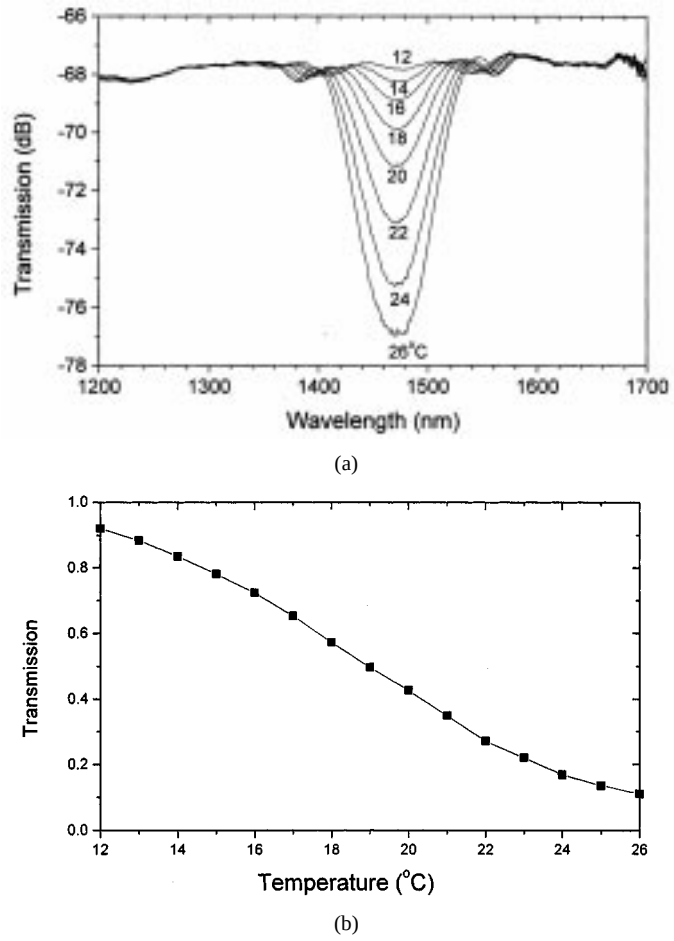

Fig. 15. Temperature sensor based on measurement of the $m = 12$ mode of a 175-μm period LPFG operated off resonance. (a) Transmission spectrum for different temperatures. (b) Transmitted intensity plotted against temperature.

Fig. 15 illustrates the response to varying temperature of the $m = 12$ cladding mode resonance of a 175-μm period LPFG. Fig. 15(a) shows the transmission spectra, and Fig. 15(b) the relative transmitted intensity as the temperature is increased from 12 °C to 26 °C in 1° steps. In this temperature range, the LPFG operated slightly off resonance. It is clear that the temperature increase has caused no distinct wavelength shift, but has induced increasing coupling to the resonance with a corresponding decrease in the transmission of the grating. The central portion of the curve of Fig. 15(b), 14 °C $\sim$24 °C, shows a near-linear response with the transmission changing from 83.6% to 16.9% across this range; the average sensitivity is -6.67% per °C, and a detector resolving 0.01% of the transmitted intensity can register a 0.002 °C temperature change.

Fig. 16 illustrates the same concept applied to the measurement of strain using, in this case, the $m = 11$ mode of a 203-μm period LPFG. For an applied strain varied from 0 $\mu\varepsilon$ to 3000 $\mu\varepsilon$, Fig. 16(a) shows the mode transmission spectra, and Fig. 16(b) the relative transmitted intensity with the sensor, again, working a short way off the resonance condition. Here, increasing strain decreases the coupling strength without detectable change in peak wavelength, and the near-linear transmitted intensity response yields an averaged sensitivity of 0.025%/$\mu\varepsilon$. In this instance, a detector capable of resolving 0.01% change in transmitted intensity yields a strain resolution of 0.4 $\mu\varepsilon$.

IV. Discussion

We have obtained very close agreement between the results of theoretical calculations and experiments for the sensitivity distributions in LPFGs as a function of the mode order for several external variables, and for the wavelengths of the turning points. We recognize some small differences between some experimentally determined wavelengths (Table I) and the theoretical predictions (Fig. 1) for some periods, and we can identify some contributory causes. First, the theoretical calculations are based on the weakly guiding approximation that predicts the dispersion of the core and cladding modes with limited accuracy. Second, the assumed boron-doping level in the simulations may not be precisely matched to that of the experimental fiber. Third, due to differing exposure times in several cases, the average value of the UV-induced δn was not constant for all gratings, as assumed in the calculations. Nevertheless, the experimental agreement with the predicted trends is close in all cases, with only relatively minor discrepancies being apparent.

It can be observed in Figs. 10, 12(b), and 13(a) that the spectral widths of the resonance peaks are broad where they are close to the turning points, and narrower where they are fur-

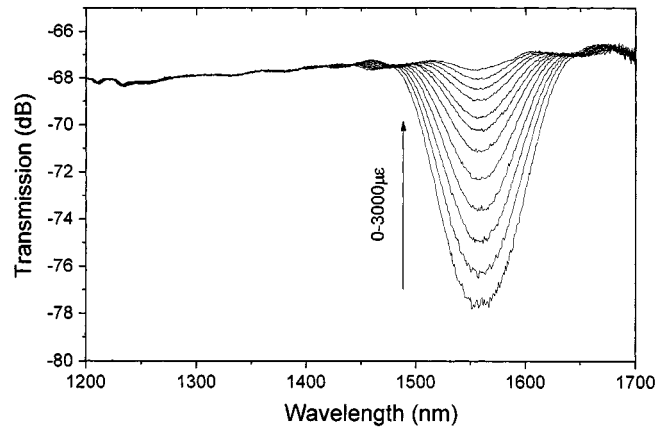

(a)

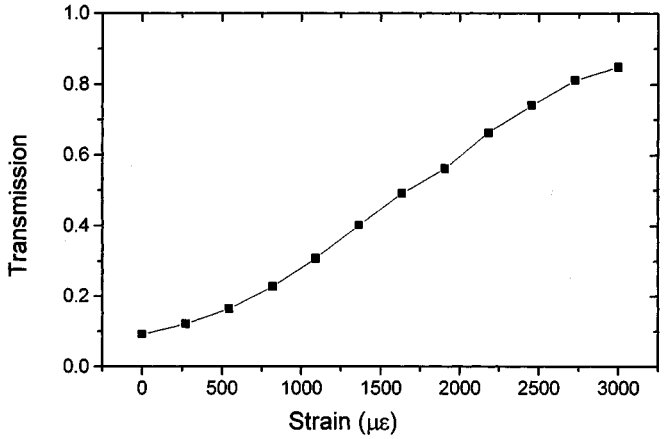

(b)

Fig. 16. Strain sensor based on measurement of the $m = 11$ mode of a 203-μm period LPFG operated off resonance. (a) Transmission spectrum for different strains. (b) Transmitted intensity plotted against strain.

ther away from them. This observation cannot be explained by the frequently used formula given by Vengsarkar *et al.* [1] for the LPFG bandwidth. The explanation is provided by considering the differential dispersion between the core and cladding modes. When this is taken into account, the 3-dB bandwidth of the resonance peak of an LPFG of length L may be derived to be

$$\Delta\lambda_{3\,\mathrm{dB}} = \frac{0.8\lambda_{\mathrm{res}}^2}{L|\Delta n_g|}. \tag{10}$$

If the difference in dispersion between the two modes is zero, i.e., if $d(\Delta n_e)/d\lambda = 0$, we obtain $\Delta n_g = \Delta n_e - \lambda$. $d(\Delta n_e)/d\lambda = \Delta n_e$, and (10) reverts to Vengsarkar's expression. Equation (10) expresses a strong dependency of the spectral width on the differential group index between the modes. The closer the resonant wavelength lies to a turning point, the smaller is the value of $|\Delta n_g|$ (see Fig. 2) and, thus, by (10), the larger is the spectral width. Using (9), we may rewrite (10) as

$$\Delta\lambda_{3\,\mathrm{dB}} = |\gamma|\frac{0.8\lambda_{\mathrm{res}}^2}{L\Delta n_e}. \tag{11}$$

It is instructive to note that (11) differs from Vengsarkar's expression by just the multiplying factor γ.

Equation (10) cannot predict the bandwidth of a resonance at the turning point since, then, $\Delta n_g = 0$. For the turning point, we derive

$$\Delta\lambda_{3\,\mathrm{dB}} = \frac{1.26\lambda_{\mathrm{res}}}{\sqrt{cL\Delta D}} \tag{12}$$

where ΔD (ps/nm/km) is the difference in dispersion between the core and cladding modes, and c is the free-space velocity of light. Equation (12) demonstrates that selection of fibers with different ΔD offers the means to control the bandwidth of the grating resonance, as has been demonstrated recently by Ramachandran *et al.* [17] in the design of broad-band mode converters for higher order mode dispersion compensators. Another potential application for broad-band LPFGs may be with cascaded gratings [3] used to form comb filters with very wideband operation, useful for future WDM systems.

The expressions given in (2)–(8) may be used to design either very sensitive or very insensitive LPFGs, according to the intended application. If an LPFG sensor is designed to operate on a mode order with a high value of γ, it may be sensitive to virtually all external perturbations at the same time. In principle, however, it is possible to eliminate cross sensitivity in many cases. For example, design of a highly sensitive strain sensor requires that $|1+\Gamma_{\mathrm{strain}}|$ be as large as possible; simultaneously, to minimize temperature cross sensitivity, Γ_{temp} should be as small as possible. These conditions require appropriate choice of core and cladding materials in producing the sensor fiber. For the ideal temperature-insensitive strain sensor, the condition $\xi_{\mathrm{co}}n_{\mathrm{co}}^{\mathrm{eff}} - \xi_{\mathrm{cl}}n_{\mathrm{cl},m}^{\mathrm{eff}} = -\alpha\Delta n_e$ should be satisfied. On the other hand, a highly sensitive temperature sensor with minimal cross sensitivity to strain requires simultaneously large Γ_{temp} and small $|1+\Gamma_{\mathrm{strain}}|$, and the core and cladding materials should be chosen to satisfy the condition $\eta_{\mathrm{co}}n_{\mathrm{co}}^{\mathrm{eff}} - \eta_{\mathrm{cl}}n_{\mathrm{cl},m}^{\mathrm{eff}} = -\Delta n_e$. Usually, such conditions can only be matched precisely for one specific mode order of the LPFG. For the refractive index sensor, elimination of cross sensitivities to both strain and temperature, if required, would demand that the conditions $\xi_{\mathrm{co}}n_{\mathrm{co}}^{\mathrm{eff}} - \xi_{\mathrm{cl}}n_{\mathrm{cl},m}^{\mathrm{eff}} = -\alpha\Delta n_e$ and $\eta_{\mathrm{co}}n_{\mathrm{co}}^{\mathrm{eff}} - \eta_{\mathrm{cl}}n_{\mathrm{cl},m}^{\mathrm{eff}} = -\Delta n_e$ be satisfied simultaneously. It should be pointed out that these considerations of fiber design for minimizing the cross sensitivity are also valid points for packaging issues of LPFG devices.

It is evident, then, that the spectral profile and sensitivity properties of the LPFG can be tailored by appropriate fiber design taking account of the dispersion and the core and cladding material constants. Availability of such novel fibers is likely to be the key to realization of the full device potentials and would, no doubt, lead to many further applications.

V. Conclusion

We have presented general analytic expressions to describe the sensitivity of LPFGs to temperature, strain, and surrounding refractive index. We have shown that the LPFG sensitivity may be characterized by a general sensitivity factor γ and by variable-specific factors Γ_{temp}, Γ_{strain}, and Γ_{sur}. The theoretical analysis has revealed that the dispersion curve for each cladding mode resonance exhibits a turning point at which the maximum LPFG sensitivity occurs, and we have defined a region by $|\gamma| >$

5, within which very high sensitivity can be obtained. Experimentally, we have studied the sensitivities of different mode orders using a series of LPFGs inscribed in B–Ge codoped fiber; we have verified the theoretical descriptions with good accuracy and have confirmed the presence of the turning points. Highly sensitive sensors for each variable have been demonstrated by operating near to the turning points using two different techniques, one based on measurement of the dual resonance characteristic, and the other based on a simple intensity measurement off-resonance. Sensitivities as high as 3.4 nm/°C and -33.6 nm/mε have been obtained with high resolution. We believe that the sensitivity values reported here are the highest yet recorded for LPFG sensors.

ACKNOWLEDGMENT

The authors wish to thank Dr. Y. Liu for useful and stimulating technical discussions.

REFERENCES

[1] A. M. Vengsarkar, P. J. Lemaire, J. B. Judkins, V. Bhatia, T. Erdogan, and J. E. Sipe, "Long-period fiber gratings as band-rejection filters," *J. Lightwave Technol.*, vol. 14, pp. 58–64, Jan. 1996.

[2] A. M. Vengsarkar, P. J. Lemaire, G. Jacobovitz-Veselka, V. Bhatia, and J. B. Judkins, "Long-period fiber gratings as gain-flattening and laser stabilizing devices," in *Proc. IOOC'95*, June 1995, PD1–2.

[3] X. J. Gu, "Wavelength-division multiplexing isolation fiber filter and light source using cascaded long-period fiber gratings," *Opt. Lett.*, vol. 23, no. 7, pp. 509–510, 1998.

[4] K. O. Hill, B. Malo, K. Vineberg, F. Bilodeau, D. Johnson, and I. Skinner, "Efficient mode conversion in telecommunication fiber using externally written gratings," *Electron. Lett.*, vol. 26, pp. 1270–1272, Aug. 1990.

[5] V. Bhatia and A. M. Vengsarkar, "Optical fiber long-period grating sensors," *Opt. Lett.*, vol. 21, no. 9, pp. 692–694, 1996.

[6] H. J. Patrick, A. D. Kersey, and F. Bucholtz, "Analysis of the response of long period fiber gratings to the external index of refraction," *J. Lightwave Technol.*, vol. 16, pp. 1606–1612, Sept. 1998.

[7] Y. Liu, L. Zhang, J. A. R. Williams, and I. Bennion, "Optical bend sensor based on measurement of resonance mode splitting of long-period fiber grating," *IEEE Photon. Technol. Lett.*, vol. 12, pp. 531–533, May 2000.

[8] L. Zhang, Y. Liu, L. Everall, J. A. R. Williams, and I. Bennion, "Design and realization of long-period grating devices in conventional and high birefringence fibers and their novel applications as fiber-optic load sensors," *IEEE J. Select. Topics Quantum Electron.*, vol. 5, pp. 1373–1379, Sept./Oct. 1999.

[9] A. A. Abramov, B. J. Eggleton, J. A. Rogers, R. P. Espindola, A. Hale, R. S. Windeler, and T. A. Strasser, "Electrically tunable efficient broad-band fiber filter," *IEEE Photon. Technol. Lett.*, vol. 11, pp. 445–447, Apr. 1999.

[10] X. Shu, X. Zhu, Q. Wang, S. Jiang, W. Shi, Z. Huang, and D. Huang, "Dual resonant peaks of LP015 cladding mode in long-period gratings," *Electron. Lett.*, vol. 35, pp. 649–651, Sept. 1999.

[11] X. Shu, X. Zhu, S. Jiang, W. Shi, and D. Huang, "High sensitivity of dual resonant peaks of long-period fiber grating to surrounding refractive index changes," *Electron. Lett.*, vol. 35, pp. 1580–1581, May 1999.

[12] X. Shu, T. Allsop, B. Gwandu, L. Zhang, and I. Bennion, "Room-temperature operation of widely tunable loss filter," *Electron. Lett.*, vol. 37, pp. 216–218, Feb. 2001.

[13] T. W. MacDougall, S. Pilevar, C. W. Haggans, and M. A. Jackson, "Generalized expression for the growth of long period gratings," *IEEE Photon. Technol. Lett.*, vol. 10, pp. 1449–1451, Oct. 1998.

[14] M. J. Adams, *An Introduction to Optical Waveguides*. New York: Wiley, 1981.

[15] V. Grubsky and J. Feinberg, "Long-period fiber gratings with variable coupling for real-time sensing applications," *Opt. Lett.*, vol. 25, no. 4, pp. 203–205, 2000.

[16] K. S. Chiang, Y. Liu, M. N. Ng, and X. Dong, "Analysis of etched long-period fiber grating and its response to external refractive index," *Electron. Lett.*, vol. 36, pp. 966–967, Apr. 2000.

[17] S. Ramachandran, M. Yan, L. Crowsar, A. Carra, P. Wisk, and R. Huff, "Large bandwith, highly efficient mode coupling using long-period gratings in dispersion tailored fibers," in *Proc. OFC'01*, 2001, MC2, pp. MC2_1–MC2_3.

Xuewen Shu was born in Hunan, China, in 1973. He received the B.S. degree in physics from Hunan Normal University, Changsha, China, in 1995, and the Ph.D. degree in optoelectronics from Huazhong University of Science and Technology, Wuhan, China, in 2000.

From 2000 to 2001, he was a visiting research fellow in Photonics Research Group at Aston University, Birmingham, U.K. In September 2001, he joined Indigo Photonics, Ltd., Birmingham, U.K. His current research interest is in the field of fiber grating technology and its applications in telecommunications and optical sensing.

Lin Zhang received the undergraduate and Master's degrees from Suzhou University, Suzhou, China, in 1978 and 1986, respectively, and the Ph.D. degree from Sussex University, Sussex, U.K., in 1990.

From 1990 to 1994, she was a Research Fellow in the Department of Physics at Sussex University working in the field of passive and active planar waveguide devices. In 1994, she joined the Photonics Research Group in the Department of Electronic Engineering at Aston University, Birmingham, U.K., and is a Lecturer. Her current research interests is in the field of fiber grating technology and its applications in telecommunications and optical sensing. She has been extensively involved in four U.K. DTI and EPSRC LINK programs and many other EPSRC-, EU-, and DERA-funded research projects. She has authored and coauthored more than 150 international standard journal and conference papers.

Dr. Zhang is a member of the Optical Society of America (OSA) and the Institute of Physics.

Ian Bennion (M'91) received degrees in electrical and electronic engineering from the University of Glasgow, Glasgow, U.K.

He spent 16 years at Plessey Research Caswell, Ltd. (previously GEC-Marconi Materials Technology, Ltd.), where he headed a department of 18 scientists and engineers carrying out research into optoelectronic devices and their applications. He is currently Professor of Electronic Engineering in the Department of Electronic Engineering at the University of Aston, Birmingham, U.K. His recent research activities have been in the fields of fiber and integrated optical components for applications in communications, signal processing, optical switching, and optical interconnects. He has been extensively involved in CEC research programs in both RACE and ESPRIT.

Dr. Bennion is a member of the Optical Society of America (OSA) and a fellow of the Institution of Electrical Engineers (IEE) and the Institute of Physics.